Supporting Information for "Ocean response in transient simulations of the last deglaciation dominated by underlying ice-sheet reconstruction and method of meltwater distribution"

Marie-Luise Kapsch[1], Uwe Mikolajewicz[1], Florian Ziemen[1,2], Clemens Schannwell[1]

[1]Max Planck Institute for Meteorology, Bundesstraße 53, 20146 Hamburg, Germany

[2]Deutsches Klimarechenzentrum GmbH, Bundesstraße 45a, 20146 Hamburg, Germany.

Contents of this file

1. Text S1: MPI-ESM-CR model versions
2. Text S2: MPI-ESM-CR evaluation
3. Figures S1 to S9

Introduction

The supporting information contains text and figures to support the findings in the main document. Text S1 contains more information on the model tuning and model versions used in this study. Text S2 puts the model simulations and versions in context to other PMIP models. All figures support the findings presented in the main text.

1. Text S1: MPI-ESM-CR model versions

The model versions used in the main manuscript differ. Model version P2 is newer than version P1. It contains a range of bug fixes and an updated model tuning. Tuning the model aimed at reducing the negative bias in southern ocean sea-ice coverage and the warm bias in Antarctic Bottom water properties. It comprises the introduction of a brine plume parametrization in the ocean component MPI-OM as well as a modification of sea-ice lead closure parameters. Changes also include the improvement of the automated topography generation scripts (e.g. improving the baroclinic exchange in shallow fjords). In the atmospheric component ECHAM6, the direct use of topographic roughness was replaced by a parameterized treatment like the one in the standard ECHAM6 model. Main tuning parameters in the atmosphere are taken from Mauritsen and Roeckner (2020) and comprise the surface value of the critical humidity profile for cloud formation (crs), the threshold between cloud water and ice (csecfrl) and the fall speed of cloud ice (cvtfall). Additionally a mean volcanic aerosol forcing was taken into account. Version P3 is equivalent to version P2 but with a slight reduction of csecfrl (from 910^{-6} to 810^{-6}) leading to a warmer climate, as temperatures for the PI (and the LGM) in P2 turned out to be too cold.

2. Text S2: MPI-ESM-CR evaluation

Fig. S1 and Fig. S2 show that the model with all its versions fits well within the range of PMIP4 models for pre-industrial (PI) climate conditions (see Kageyama et al. (2020) for a comprehensive evaluation of the PMIP4 models used for comparison). Global mean temperatures lie between 13.6°C and 14.0°C for the MPI-ESM simulations and between 12.6°C and 15°C for the PMIP4 ensemble. The LGM temperatures of the PMIP4 ensemble

range between 7.4 and 11.0°C. For the MPI-ESM simulations only Ice6G_P1, Glac1D_P1 and the Ice6G_P3 simulation fall within this range. The other model simulations are colder during the LGM, down to 6.4°C for the Glac1D_P2 simulation. Locally, the largest discrepancies between Glac1D_P2 and the PMIP4 ensemble during the LGM are evident in the Southern Hemisphere, specifically South America, South Africa and over the Pacific and Indian ocean Fig. S2. Differences are also evident over the North Atlantic, indicating the importance of the boundary conditions for the global near-surface air temperatures, as discussed in the main document. The temperature difference between LGM and PI (LGM-PI) is largest for model versions P2 and P3 and falls out of the range of the PMIP4 models for the simulations with GLAC-1D ice sheets. For P2 and P3, LGM-PI temperature anomalies are about 1°C colder for the simulations with GLAC-1D ice sheets as compared to the simulations with Ice6G ice sheets. This indicates a significant impact of the ice sheet boundary conditions on the modeled climate response.

The spread of global mean precipitation is significantly larger in the PMIP4 models than for the experiments conducted with MPI-ESM-CR. The LGM and PI global mean precipitation lies within the range of PMIP4 models. However, similar to the temperature, precipitation changes between LGM and PI in Glac1D_P2 and Glac1D_P3 are larger than in the other simulations. This, again, emphasizes how important ice sheet boundary conditions are for the climate state.

References

Kageyama, M., Harrison, S. P., Kapsch, M.-L., Löfverström, M., Lora, J. M., Mikolajewicz, U., ... Volodin, E. (2020). The PMIP4-CMIP6 Last Glacial Maximum

experiments: preliminary results and comparison with the PMIP3-CMIP5 simulations. *Climate of the Past Discussions*, *2020*, 1–37. Retrieved from https://cp.copernicus.org/preprints/cp-2019-169/ doi: 10.5194/cp-2019-169

Löfverström, M., & Lora, J. M. (2017). Abrupt regime shifts in the North Atlantic atmospheric circulation over the last deglaciation. *Geophysical Research Letters*, *44*(15), 8047-8055. Retrieved from https://agupubs.onlinelibrary.wiley.com/doi/abs/10.1002/2017GL074274 doi: https://doi.org/10.1002/2017GL074274

Mauritsen, T., & Roeckner, E. (2020). Tuning the mpi-esm1.2 global climate model to improve the match with instrumental record warming by lowering its climate sensitivity. *Journal of Advances in Modeling Earth Systems*, *12*(5), e2019MS002037. Retrieved from https://agupubs.onlinelibrary.wiley.com/doi/abs/10.1029/2019MS002037 (e2019MS002037 10.1029/2019MS002037) doi: https://doi.org/10.1029/2019MS002037

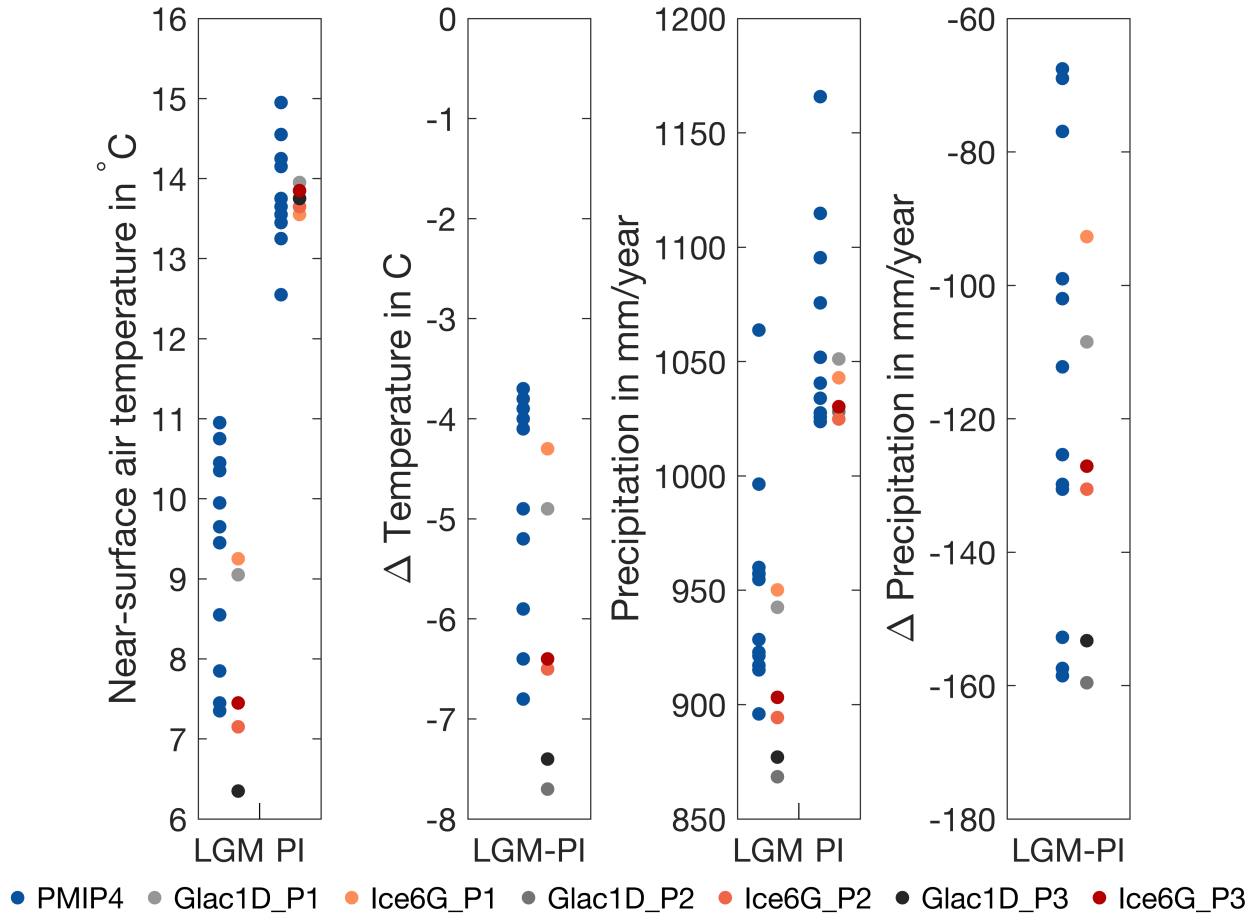

Figure S1. Global mean near-surface air temperature and precipitation for LGM and PI conditions as well as the difference between LGM and PI for the model experiments conducted for this study and a PMIP4 ensemble. Colors indicate the MPI-ESM model simulations. The PMIP4 model ensemble includes AWIESM1, AWIESM2, CCSM4-UofT, CESM1-2, HadCM3-Glac1D, HadCM3-Ice6GC, INM-CM4-8, MPI-ESM1.2-LR, MIROC-ES2L, IPSLCM5A2, iLOVECLIM1-1-1_Glac1D, iLOVECLIM1-1-1_Ice6GC (see Kageyama et al. (2020) for a detailed list of the model simulations). Note that the runs of this study are offset from the PMIP4 simulations along the x-axis for ease of interpretation.

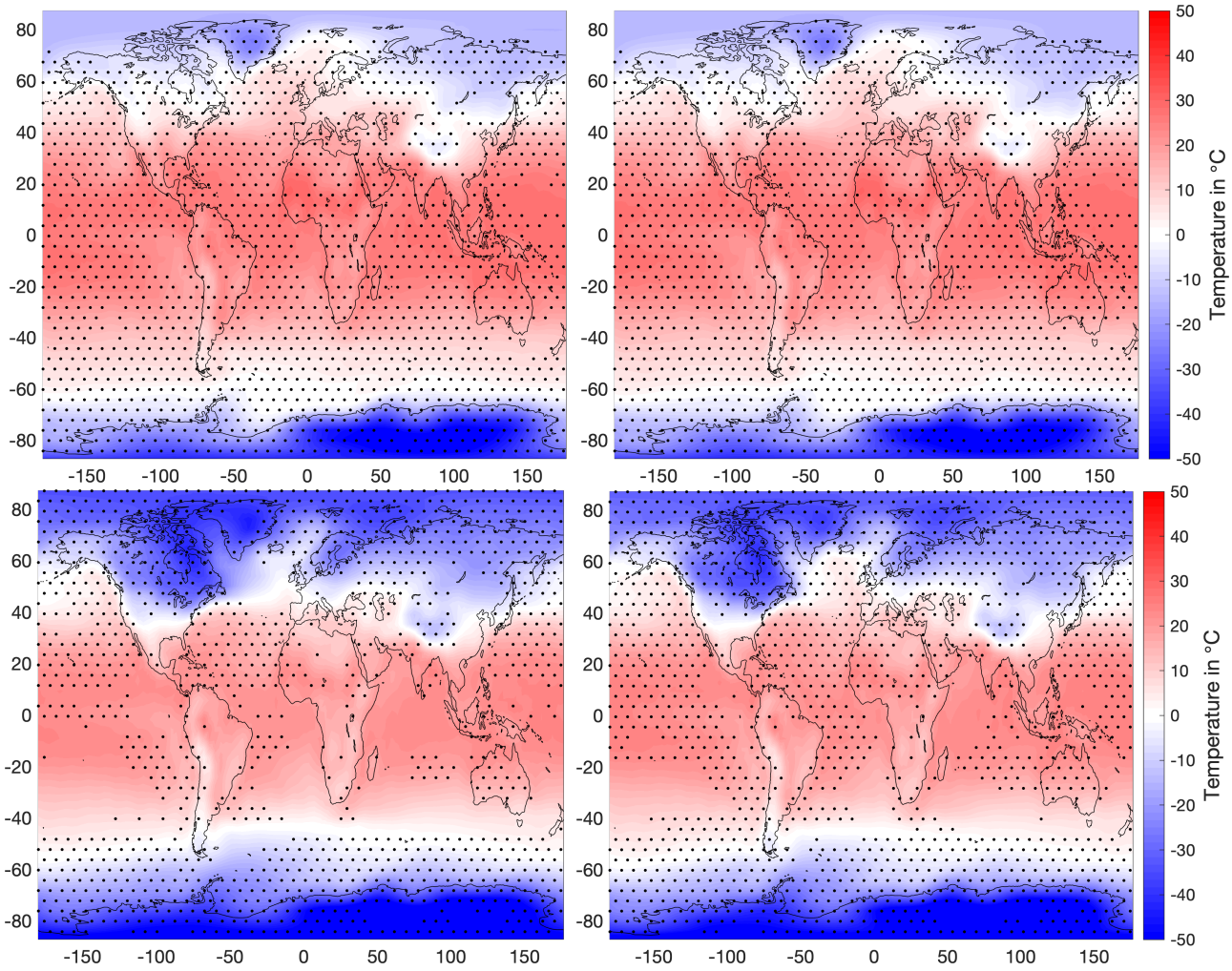

Figure S2. Near-surface air temperature for PI (top) and LGM (bottom) for the simulations Glac1D_P2 (left) and Ice6G_P2 (right). Stippling indicates where values lie within the range of the PMIP4 models introduced in Fig S1.

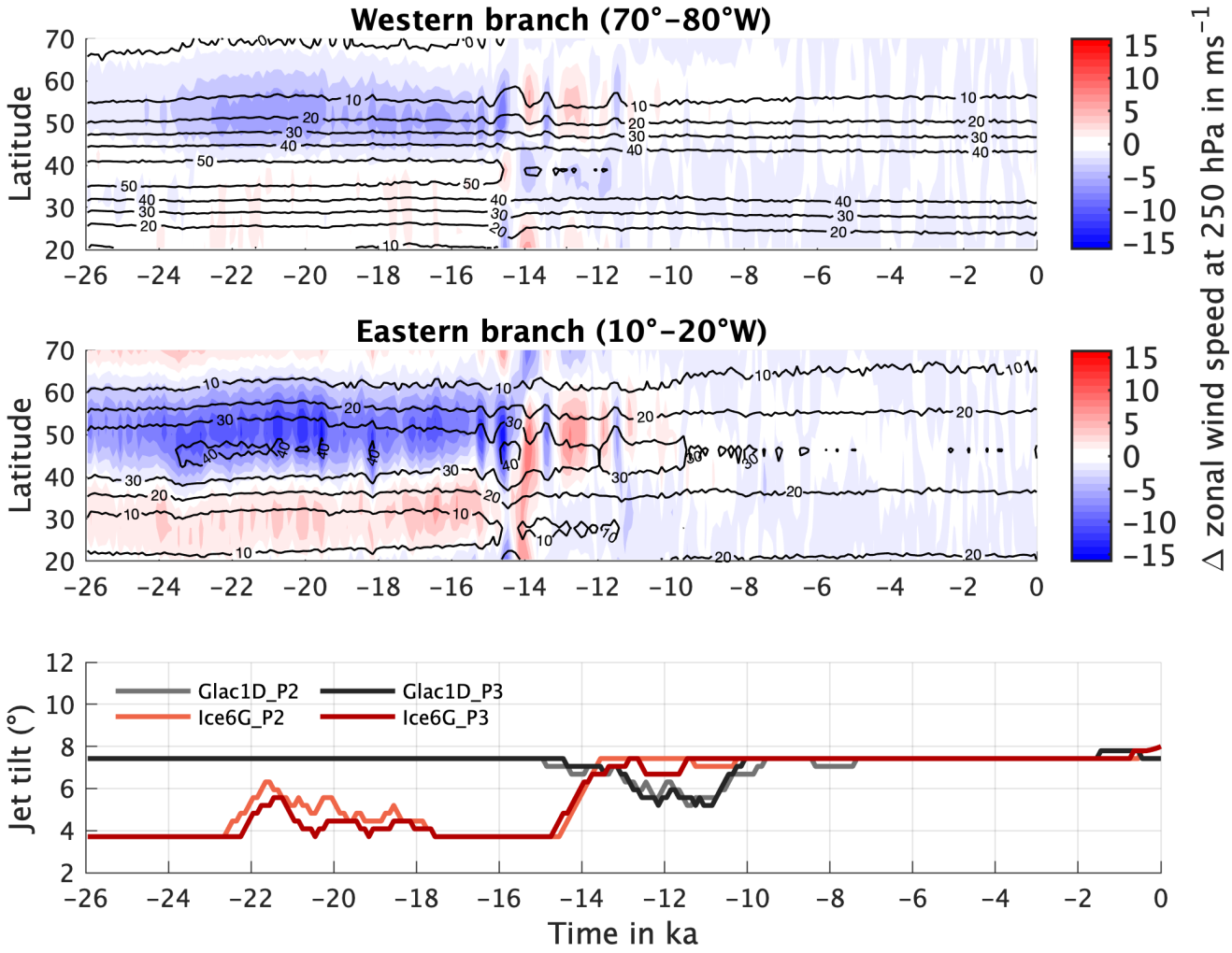

Figure S3. Zonal wind speed difference for Ice6G_P2 and Glac1D_P2 and jet stream tilt for Ice6G_P2, Glac1D_P2, Ice6G_P3, Glac1D_P3. Difference in the zonal wind speed between Ice6G_P2 and Glac1D_P2 over the western (70°W and 80°W) and eastern (10°W–20°W) North Atlantic, respectively (top panels). Contours show the zonal wind speed for the Glac1D_P2 experiment. Jet tilt as calculated from the latitudinal difference of the western and eastern jet branch (bottom panel). Note, that the jet tilt is very similar in P2 and P3 and partly overlaps. Analysis is based on Löfverström and Lora (2017). The jet tilt is smoothed using a moving average with a window length of 10 time steps (1000 years).

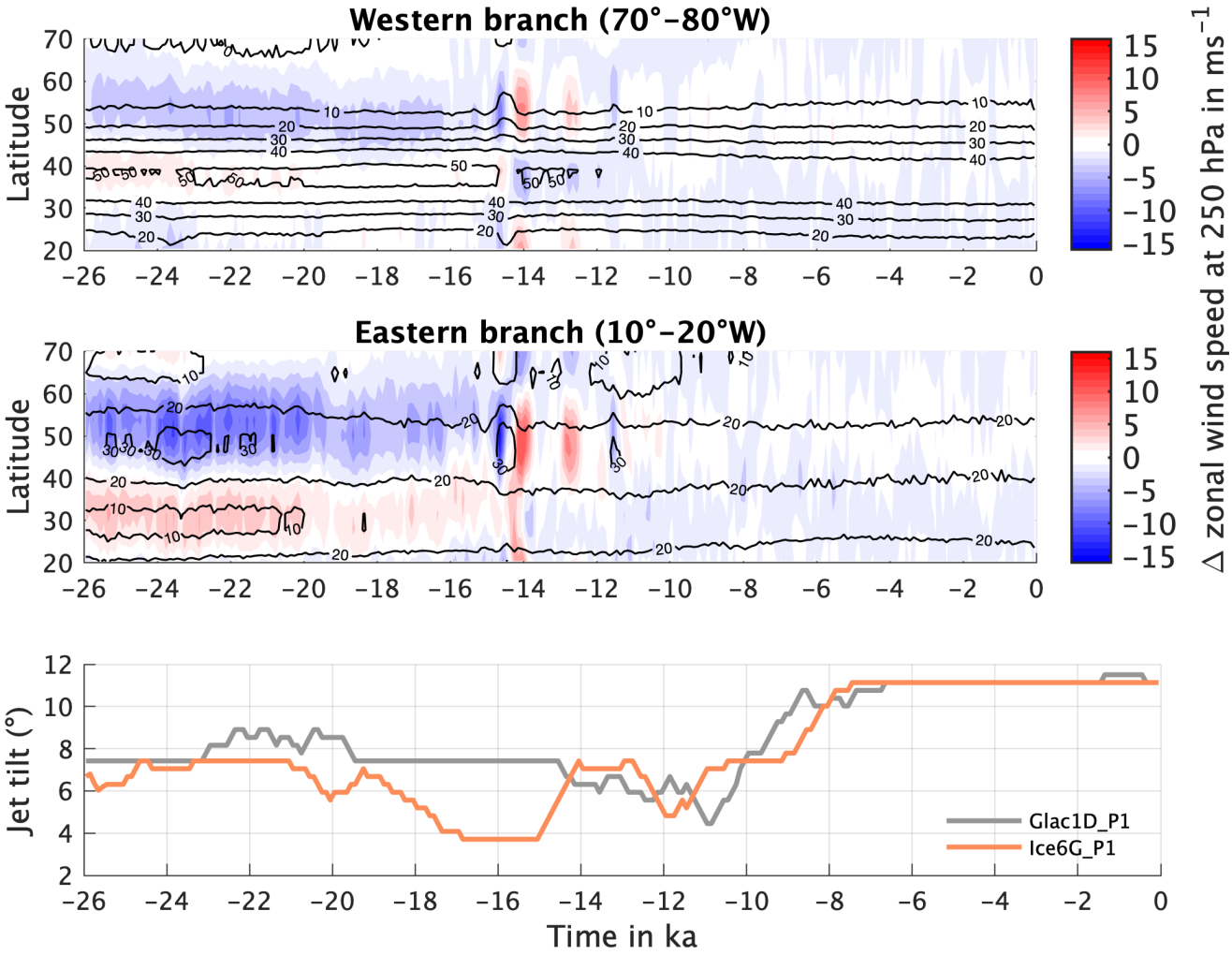

Figure S4. Similar to Fig. S3 but for Ice6G_P1 and Glac1D_P1.

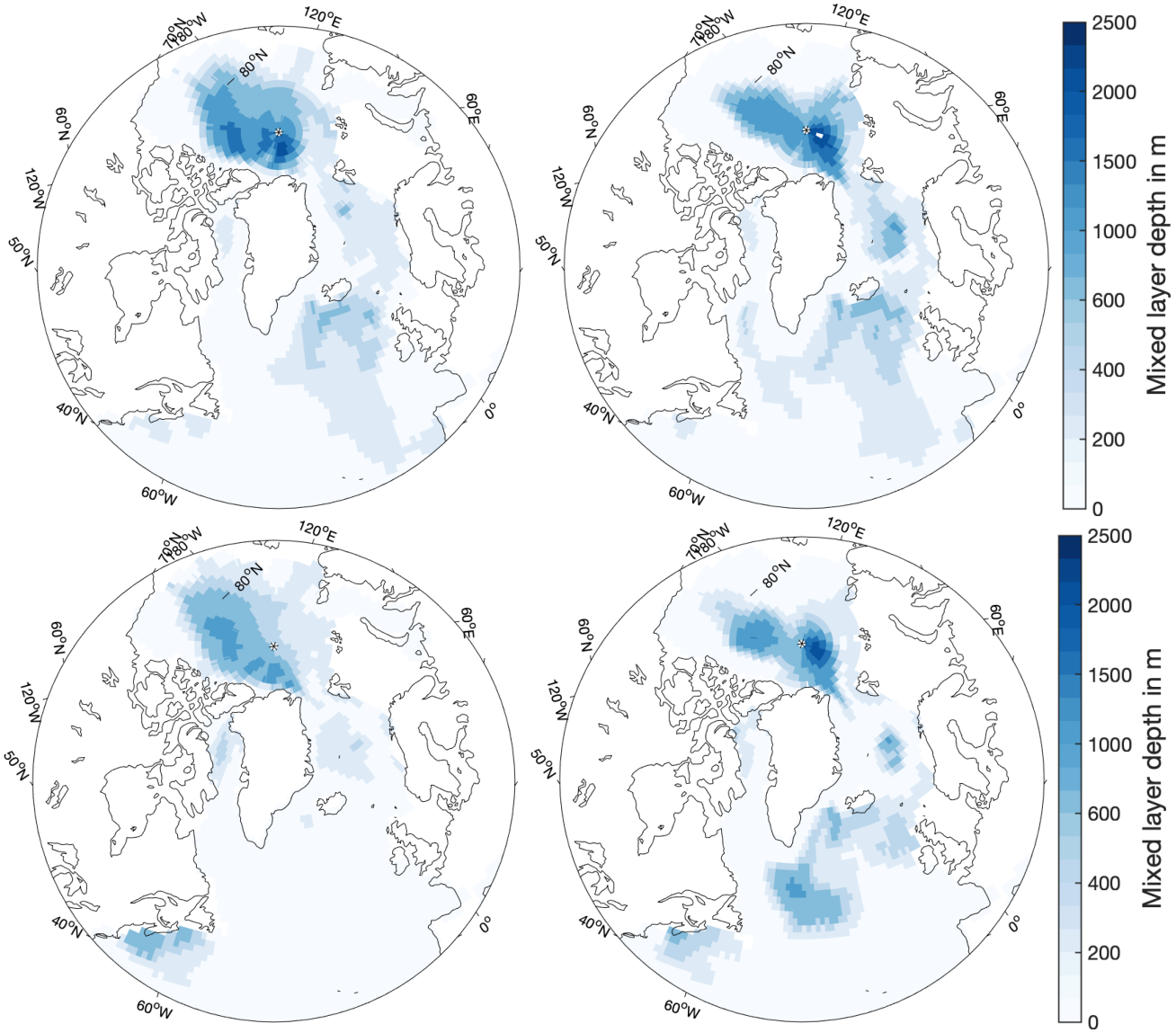

Figure S5. LGM mixed layer depth for model versions P1 (top) and P2 (bottom) with GLAC-1D (left) and ICE-6G (right) boundary conditions.

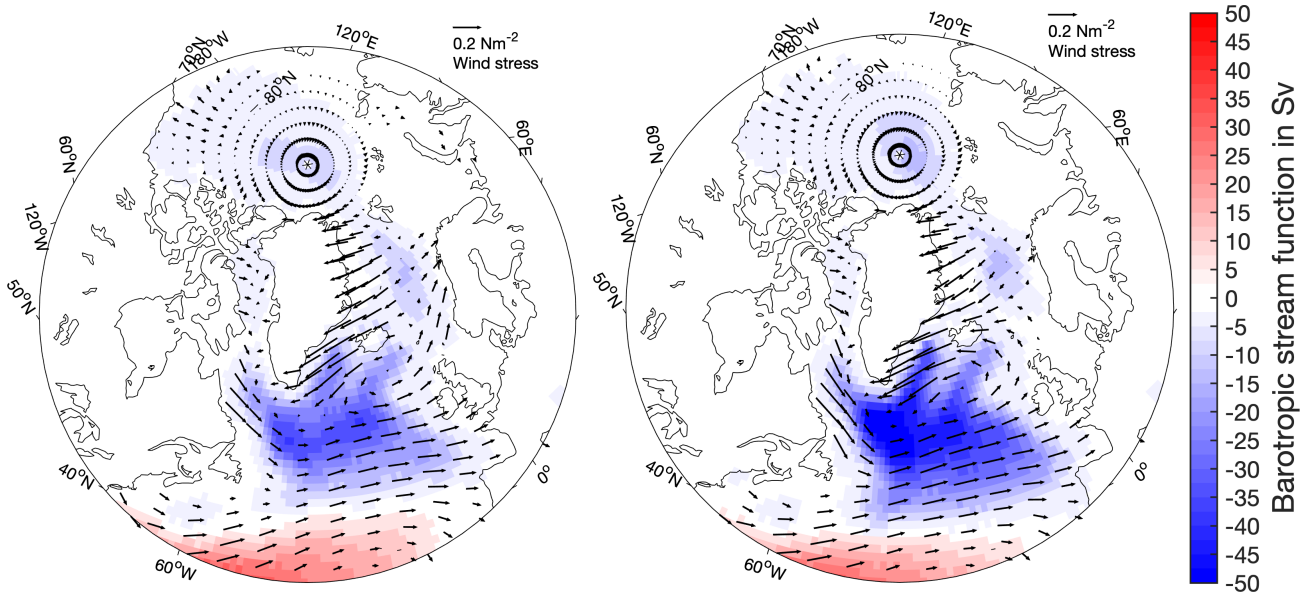

Figure S6. LGM barotropic stream function for Glac1D_P2 (left) and Ice6G_P2 (right) ice sheets. Arrows show the surface wind stress.

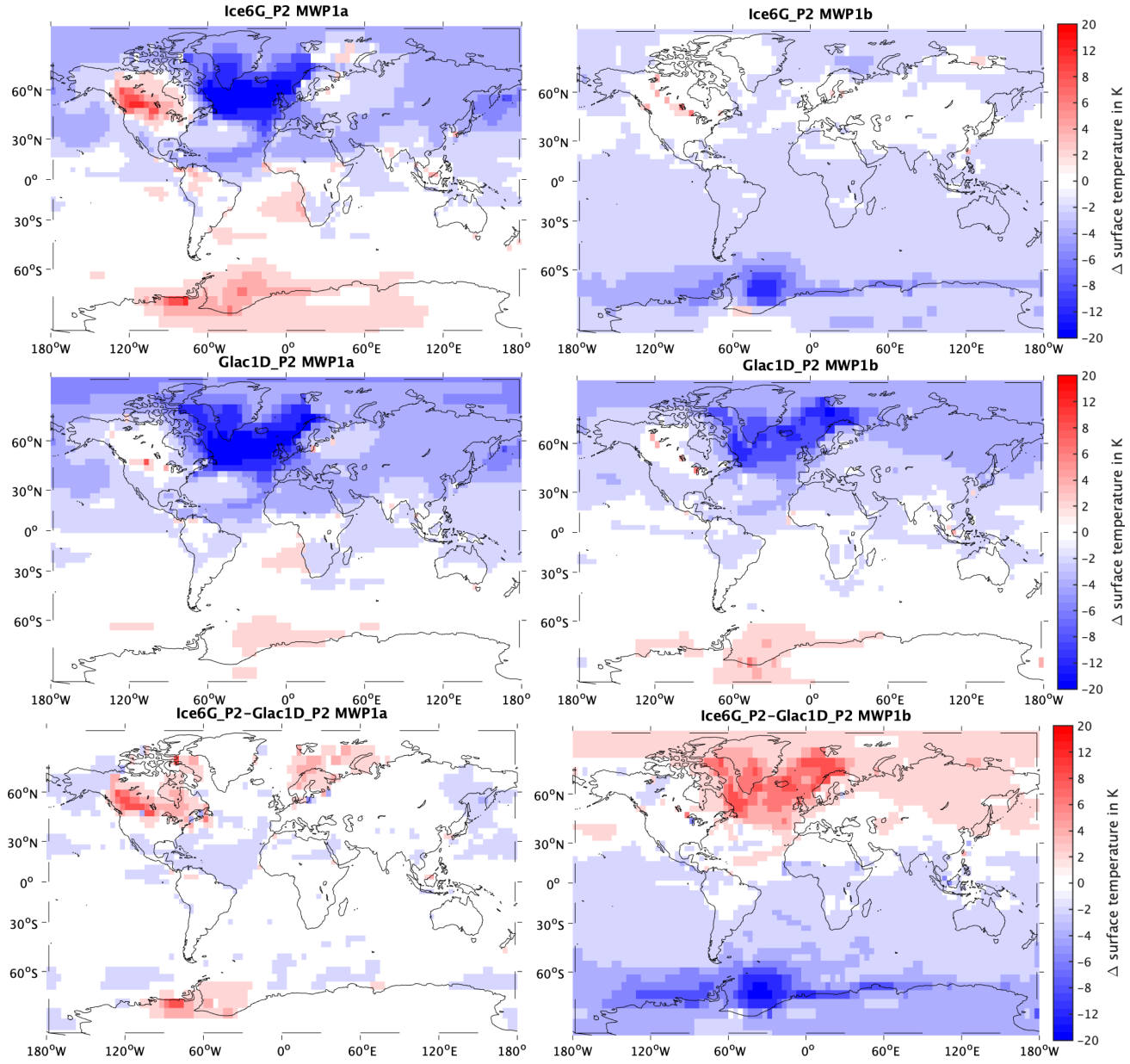

Figure S7. Temperature response due to MWP1a (left) and MWP1b (right) in Ice6G_P2 (top) and Glac1D_P2 (center) as well as the differences between the two. Note the different timing of the events (see Fig. 1, main text).

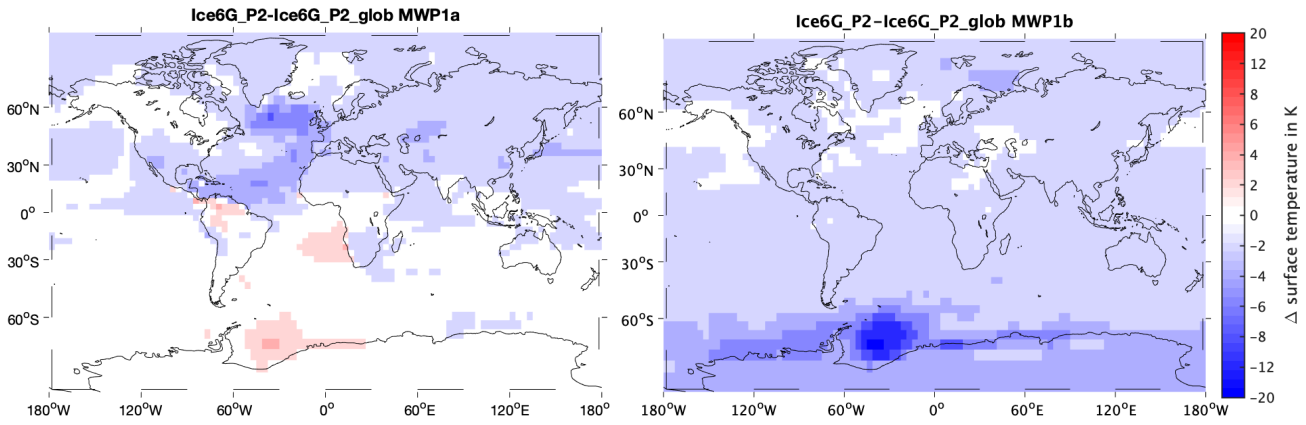

Figure S8. Difference in temperature response to MWP1a (left) and MWP1b (right) between Ice6G_P2 and Ice6G_P2_glob.

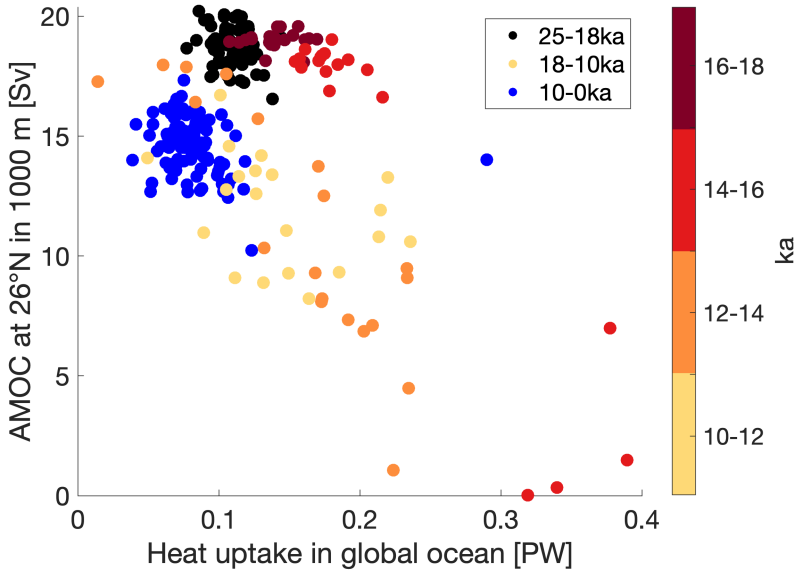

Figure S9. Scatter plot of AMOC vs. global ocean heat uptake in Ice6G_P2. Colors indicate the periods from 25-18 ka (black), 18-10 ka (yellow to red) and 10-0 ka (blue). The period 18-10 ka is subdivided into sub-periods, which are referred to in the color bar. Specifically during times when the CO_2 concentration increases rapidly, a non-linear relationship between heat uptake and the AMOC is evident. This non-linearity is most relevant between 12 and 16 ka.